Post-Print

The final publication is available at https://doi.org/10.1016/j.renene.2014.07.048

Access to the published version may require subscription.

When citing this work, cite the original published paper.

Permanent link to this version
http://hdl.handle.net/11311/868401

Validation of a wind misalignment observer using field test data[†]

C.L. Bottasso[*,a,b], C.E.D. Riboldi[b]

[a]*Wind Energy Institute, Technische Universität München, Boltzmannstraße 15, D-85748 Garching, Germany*
[b]*Dipartimento di Scienze e Tecnologie Aerospaziali, Politecnico di Milano, Via La Masa 34, Milano, I-20156 Italy*

Abstract

A previously described observer of wind misalignment is validated using field test data collected on the NREL CART3 wind turbine. The observer uses blade root bending moment 1P harmonics, computed using the transformation of Coleman and Feingold, to infer the rotor-equivalent relative wind direction. The observation model parameters are determined by a least squares fitting using recorded blade loads and met-mast measured wind direction and speed; a random sample consensus (RANSAC) algorithm is used to robustify the parameter estimation procedure while detecting outliers in the experimental samples. The observer is validated using an independent verification data set: recorded blade bending loads are fed to the observer and the estimated wind misalignment is compared to both the one provided by the met-mast vanes, assumed as the ground truth, and by an on-board nacelle-mounted wind vane. Results show that the rotor-equivalent wind misalignment estimates provided by the proposed observer are well correlated in the low frequency spectrum with the met-mast reference, and in general in much better accordance with it than the on-board wind vane measurements.

Key words:

Wind observer, Wind misalignment, Wind turbine control, Aeroelasticity, Field testing

Notation

e_i	Misalignment observation error for the ith time sample
f	Frequency
m	Blade bending moment
C_{xy}	Coherence between signals x and y
E_p	Normalized misalignment observation error increase for the pth perturbation type
P_{xy}	Power spectral density of signals x and y
V	Wind speed

[*]Corresponding author, *Tel.:* +49-89-289-16353; *Fax:* +49-89-289-16354.
Email address: `carlo.bottasso@tum.de` (C.L. Bottasso)

$\boldsymbol{a}$	Vector of observation model parameters
$\boldsymbol{m}$	Vector of blade moment driving inputs
$\boldsymbol{w}$	Vector of measured wind misalignments
$\boldsymbol{M}$	Matrix of measured driving inputs
$\mathcal{C}$	Consensus set
$\mathcal{I}$	Identification data set
$\mathcal{V}$	Verification data set
β	Blade flap angle
ψ	Azimuth angle
φ	Misalignment angle
Ω	Rotor angular speed
$(\cdot)^*$	Observed quantity
$(\cdot)^T$	Transpose
$(\cdot)^{\mathrm{IP}}$	Rotor in-plane component
$(\cdot)^{\mathrm{OP}}$	Rotor out-of-plane component
$(\cdot)^{\mathrm{wv}}$	Wind vane measured quantity
$(\cdot)_b$	Quantity pertaining to blade b
$(\cdot)_k$	Quantity pertaining to the kth wind speed
$(\cdot)_n$	Nominal (unperturbed) quantity
$(\cdot)_p$	Quantity pertaining to the pth perturbation case
$(\cdot)_{1c}$	First cosine harmonic
$(\cdot)_{1s}$	First sine harmonic
$\bar{(\cdot)}$	Average quantity
$\hat{(\cdot)}$	Filtered quantity
$\tilde{(\cdot)}$	Normalized quantity
FBG	Fiber Bragg grating
LPV	Linear parameter varying
LQR	Linear quadratic regulator
RANSAC	Random sample consensus

1. Introduction

Reliable information about the misalignment of the wind with respect to the rotor of a wind turbine is important because of a number of reasons. In fact, wind misalignment reduces power capture and may

increase loading and fatigue. Furthermore, the realignment into the wind of the rotor-nacelle assembly of a modern multi-MW machine implies the motion of a very massive structure, which should then be driven by accurate and reliable information about the wind direction.

Wind misalignment is routinely measured on-board wind turbines by local sensors, often represented by wind vanes placed on the nacelle. Such sensors are possibly disturbed by the rotor wake and by the three-dimensional flow around the nacelle. Furthermore, they invariably provide a local information at a point in proximity of the nacelle, information that may bear little resemblance to the actual distribution of wind direction over the rotor disk, which may span an area of very considerable diameter.

To overcome the limits of existing wind direction sensors, a wind misalignment observer was described in Ref. [1]. The observer uses blade bending moments, as measured by strain gages or fiber Bragg grating (FBG) optical sensors, to infer the rotor-equivalent wind misalignment. In fact, a misalignment of the wind with respect to the rotor affects the aeroelastic response of the blades; exploiting this fact, by simply looking at the lowest one-per-rev (or 1P) harmonics of the blade loads, one may estimate the wind direction relative to the rotor. In contrast to existing sensors, such as wind vanes, the information provided by the observer represents the effective wind direction felt by the rotor, which is in fact the quantity that should be used for driving realignment strategies and that is clearly superior to any local point measure, especially on very large rotors.

The structure of the observer described in Ref. [1] was suggested by the analysis of a simple analytical flapping blade model. For a better fidelity of the observer, however, the actual parameters of the model were not the ones obtained from the analytical model, but were rather based on an estimation approach. This process can be conducted either using an aeroelastic model of the machine (model-based approach) to simulate its response, or directly using data collected on the target wind turbine (model-free approach). As the former relies on a model of the machine, any imprecision in the same model may pollute the estimates provided by the observer. The latter approach avoids this problem by not relying on a model, but necessitates of field test data of sufficient quality and informational content to allow for the synthesis of the observation model so as to cover the entire operating regime of interest. Reference [1] demonstrated both approaches, the model-based one using a high-fidelity aeroelastic model of a multi-MW machine, and the model-free one using an aeroelastically-scaled wind tunnel model.

The main goal of this paper is the demonstration and validation of the wind misalignment observer using the model-free approach based on field test data collected on the Control Advanced Research Turbine (CART3) of the National Renewable Energy Laboratory (NREL), described in Refs. [3, 4], and the development of the necessary data processing algorithms. The machine is equipped with blade load sensors and an on-board wind vane; furthermore, a met-mast provides for the measurement of wind speed and direction at three different altitudes above ground.

3

Prior to the analysis using the experimental data, an investigation is conducted using a high-fidelity simulation model aimed at verifying the robustness of the observer in the face of perturbations of some of the parameters of the wind turbine, including foundation characteristics, orographic effects on the wind vertical direction, airfoil aerodynamics, rotor unbalance and blade sensor miscalibration, all quantities that may easily change between one installation and the other of a same wind turbine version. Results indicate that the observer is robust to such parameter changes; this is mainly due to the fact that the observer formulation uses only the low-frequency (1P) response of the rotor, a quantity that is little affected by small changes in the wind turbine characteristics. Therefore, one may think of calibrating the observer using a machine equipped with a met-mast (or equivalent sensor), and then use the same observer on-board other installations of the same version of that machine; this also implies that re-calibration of the observer during the lifetime of each wind turbine is probably unnecessary.

After this study, a first experimental data set is used for the synthesis of the observation model: met-mast measured wind directions and associated blade load harmonics computed by the transformation of Coleman and Feingold (see Ref. [6]) are used for the least squares fitting of various models at varying wind speeds, leading to a linear parameter varying (LPV) wind scheduled observation model covering the entire range of wind speeds of interest. Given the level of noise and turbulence in the data set, as well as because of the presence of outliers, a two stage procedure is developed to robustify the identification process. At first, candidate time sequences are identified where the wind conditions and the response of the machine are sufficiently constant for a sufficient length of time. Next, outliers in the time sequences are discarded by using a random sample consensus (RANSAC, cf. Ref. [7]) algorithm. The results reported in this work are limited to the partial and full load regimes, as the analysis of the available data sets in the transition region around rated wind speed revealed a large number of outliers, making the selection of suitable time sequences difficult and the identification results quite unreliable.

Having identified the observation model, a second independent data set is used for the validation of the observer. Here again, a similar two stage procedure is used for selecting suitable time sequences and for discarding outliers. Results show that the proposed observer is in general better correlated with the met-mast reference than the wind vane, supporting the initial hypothesis that the point information provided by the standard sensor may often be grossly in error. Furthermore, the observed wind misalignment time histories appear to match well the met-mast ones in the lowest frequency spectrum, which is the one used for driving yaw control strategies on-board wind turbines, as the machine is in fact actually yawed only when the misalignment has been sufficiently large for a sufficient length of time. Conclusions on the results of the present study are given in the final section.

2. Wind misalignment observer formulation

2.1. Observation model

An observer for rotor-flow misalignment and vertical shear using blade root loads was presented in Ref. [1] and it is briefly reviewed here. The structure of the observer is based on the analytical model of the flapping blade, as presented in Ref. [8], while the actual model coefficients are obtained by a process of parameter estimation. We consider here the sole observation of wind misalignment in non-yawing conditions; the more general case that includes the vertical wind shear and a steady state yawing maneuver are analyzed in Ref. [1].

The model structure is found by considering a flapping rigid blade, connected to the hub by an elastic hinge; hub off-set and hinge stiffness are tuned to represent the blade first natural mode of motion and its frequency. The structural blade representation is complemented by an aerodynamic model that computes the lift and drag at each blade station, by considering the effects of blade rotation and flapping motion, of the induced velocity, and of the wind intensity, direction and vertical shear. One assumes steady wind conditions and a resulting periodic response of the blade, which, truncating the blade flapping angle β at the 1P harmonic, is expressed as

$$\beta = \beta_0 + \beta_{1c} \cos \psi + \beta_{1s} \sin \psi, \tag{1}$$

where ψ is the blade azimuthal angle. Next, by substitution of the truncated blade response in the flap equation of motion, dropping higher order terms in the process, one can express the coning β_0 and the two cyclic terms β_{1c} and β_{1s} as functions of the wind parameters (speed, misalignment and shear).

The crucial observation of Ref. [1] is that this linear relationship can be inverted. Hence, one can compute the wind misalignment (and vertical shear), from the sole knowledge of the blade 1P harmonics. Replacing the flap angle with the easier to measure out-of-the-rotor-plane blade root bending moments, and adding the rotor-in-plane bending moments as well for increased observability (cf. Ref. [1]), one finally gets the observation model in the form

$$\varphi = \boldsymbol{a}(V)^T \boldsymbol{m}. \tag{2}$$

The wind misalignment angle $\varphi \in [-\pi/2, \pi/2]$ is defined as $\varphi = \varphi_{\text{wind}} - \varphi_{\text{nacelle}}$, where φ_{wind} is the absolute wind direction, measured with respect to the North and positive when coming from the East, and φ_{nacelle} is the absolute direction of the nacelle. Furthermore, $\boldsymbol{a}$ is a vector of coefficients, which are scheduled in terms of the mean rotor-equivalent wind speed V, while $\boldsymbol{m}$ is the driving input vector of load harmonics

$$\boldsymbol{m} = (m_{1c}^{\text{OP}}, m_{1s}^{\text{OP}}, m_{1c}^{\text{IP}}, m_{1s}^{\text{IP}})^T, \tag{3}$$

where out and in-plane components are noted $(\cdot)^{\text{OP}}$ and $(\cdot)^{\text{IP}}$, respectively.

The coefficients $\boldsymbol{a}$ suggested by the analytical model are not used in practice, as the model is rather crude and only serves the purpose of understanding the physics and suggesting the model structure. Coefficients $\boldsymbol{a}$

in model (2) are then considered as unknown, and must be derived by a process of identification from known wind inputs and associated blade responses, as described later on.

Reference [1] showed that the least variability in the model coefficients $\boldsymbol{a}$ is obtained by normalizing the driving input vector $\boldsymbol{m}$ by the zeroth harmonic, i.e. by using m_{1c}/m_0 and m_{1s}/m_0. This was avoided here, because inaccurate calibration or drifting of the load sensors may affect m_0 thereby polluting the wind misalignment estimates. The present choice implies a slightly increased variability of the model coefficients with wind speed, which is simply addressed by using a larger number of wind speeds at which coefficients are pre-computed for later model interpolation during run time scheduling.

2.2. Model synthesis and interpolation

A process of parameter estimation is used in order to find the unknown coefficients $\boldsymbol{a}$ in Eq. (2). Wind direction and speed are measured just upstream of the rotor by a suitable instrument, as for example a met-mast. Furthermore, bending moments in the flap and lag directions at the root of each blade are measured by strain gages or FBG optical sensors, and transformed into out and in-plane rotor components based on the blade pitch attitude.

The bending moment lowest harmonic amplitudes m_{1c} and m_{1s} are computed at each instant in time by the transformation of Coleman and Feingold (see Ref. [6]), which writes

$$
\left\{
\begin{array}{c}
m_{1c} \\
m_{1s}
\end{array}
\right\}
= \frac{2}{3}
\left[
\begin{array}{ccc}
\cos \psi_1 & \cos \psi_2 & \cos \psi_3 \\
\sin \psi_1 & \sin \psi_2 & \sin \psi_3
\end{array}
\right]
\left\{
\begin{array}{c}
m_1 \\
m_2 \\
m_3
\end{array}
\right\},
\tag{4}
$$

where ψ_b is the azimuth of the bth blade, and m_b the corresponding out or in-plane bending moment component. A zero-phase low-pass fourth-order Butterworth filter is used to remove undesired disturbances at 3P and above in the Coleman-transformed harmonic amplitudes (see Ref. [9]).

The identification is based on a set of samples, including wind misalignment and speed, and associated 1P harmonic loads, each sample corresponding to a given time instant t_i. In order to account for the variability of the observer coefficients with respect to wind speed, different models are identified for different pre-selected wind speeds V_k in the operating range of the machine; such models are then interpolated at run time as explained later on to obtain a LPV observation model.

To select samples based on wind speed, at first a mean wind speed estimate $\hat{V}$ is generated by filtering with a 5 sec moving average the instantaneous wind speed measurements. Next, misalignment and load samples are assigned to the corresponding wind speed bucket if their filtered velocity satisfies $\hat{V}_i \in [V_k - \Delta V, V_k + \Delta V]$, where ΔV is the half bucket amplitude. This defines the set of samples used for identification at the kth wind speed as $\mathcal{I}_k = \{\varphi_i, \boldsymbol{m}_i, i = 1, \ldots, N_{\mathcal{I}_k} \mid \hat{V}_i \in [V_k - \Delta V, V_k + \Delta V]\}$, where $N_{\mathcal{I}_k}$ is the number of samples in that set.

Using Eq. (2) and collecting together all samples within set k, one gets

$$\boldsymbol{w}_k = \boldsymbol{M}_k^T \boldsymbol{a}(V_k), \tag{5}$$

where

$$\boldsymbol{w}_k = (\varphi_1, \varphi_2, \ldots, \varphi_{N_{\mathcal{I}_k}})^T, \tag{6a}$$

$$\boldsymbol{M}_k = \left[\boldsymbol{m}_1, \boldsymbol{m}_2, \ldots, \boldsymbol{m}_{N_{\mathcal{I}_k}} \right]. \tag{6b}$$

Solving for the unknown model coefficients by least squares gives

$$\boldsymbol{a}(V_k) = \left(\boldsymbol{M}_k \boldsymbol{M}_k^T \right)^{-1} \boldsymbol{M}_k \boldsymbol{w}_k. \tag{7}$$

Once the identification has been completed over the considered range of wind speeds, so that $\boldsymbol{a}(V_k)$ is known for all the reference wind speeds V_k of interest, the observer is used at run time as follows. A mean wind speed estimate $\hat{V}$ is generated by filtering the wind turbine instantaneous wind speed measurement, obtained by the on-board anemometer or, preferably, by a wind speed observer (see Refs. [10, 11, 12]). At the generic time instant t_i, the bucket containing the current mean wind estimate $\hat{V}_i$ is found by determining k such that $\hat{V}_i \in [V_k, V_{k+1}]$. Finally, the instantaneous model coefficients are computed by linear interpolation as

$$\boldsymbol{a}(\hat{V}_i) = (1 - \xi)\boldsymbol{a}(V_k) + \xi \boldsymbol{a}(V_{k+1}), \tag{8}$$

where $\xi = (\hat{V}_i - V_k)/(V_{k+1} - V_k)$.

The run-time interpolation of the observation model coefficients is needed because of their variability with respect to wind speed. However, it is important to remark that one needs only to follow the average wind speed around which the machine is operating, similarly to what is commonly done in the scheduling of control gains [13]. In this sense, $\hat{V}$ must not be an accurate instantaneous value of the wind speed (which would be very difficult to obtain in a reliable manner), but only a reasonable estimate of the average wind speed, a quantity that in general can be obtained with good accuracy. To this end, the use of a wind speed observer is particularly recommended because it provides for a rotor-effective estimate, as filtered by the response of the machine. Extensive testing has showed that, because of the way this piece of information is used in the overall misalignment observation algorithm and because of the rather mild variation of the observer coefficients with wind speed, the performance of the observer is quite robust with respect to wind speed scheduling as long as $\hat{V}$ is capable of tracking changes in the set point around which the machine is operating.

2.3. Robustness of the estimator

As explained before, the synthesis of the observation model by the model-free approach requires synchronized wind measurements (provided by a met-mast or equivalent sensor) and blade bending loads. However,

the met-mast will not in general be available on all machines, but only on selected wind turbines used for calibration and testing activities. Therefore, one is faced with the problem of ensuring the correct operation of the observer for machines other than the met-mast equipped ones.

As the method described here uses only the 1P amplitude of the response, it is reasonable not to expect a significant variability of this harmonic amplitude across different machines of the same version; clearly, the situation would be more delicate with a more complex observer based on a wider spectrum of the machine response. If the 1P response due to misalignment changes little from one machine to the other of a same version, then one could perform the model identification on a machine equipped with a met-mast, and subsequently use the same observer on other wind turbines of that same version.

A related problem is the possible drift of some characteristics of the machine with time, as these may also in principle affect the quality of the estimates provided by the observer.

Both problems can be studied by considering the robustness of the observer in the face of perturbations of some wind turbine model parameters. If the observer is sufficiently robust, in the sense that its performance is not significantly affected by such parameter changes, then it will be applicable to different installations of a same wind turbine model and it will accompany each machine along its lifetime.

In order to investigate the robustness of the observer for both of the aforementioned important problems, a simulation study was conducted by considering the same 3MW horizontal-axis three-bladed wind turbine used in Ref. [1]. The machine was modeled in `Cp-Lambda`, a finite element multibody wind turbine simulator [14, 15], and the model included flexible blades, tower and drive-train/nacelle system, compliant foundations, and a classical BEM aerodynamic model enhanced with tip, hub and unsteady corrections, dynamic stall and tower-interference models. This variable-speed machine was regulated by a collective-pitch/torque controller based on a speed-scheduled linear quadratic regulator (LQR) with integral state [13].

The observer model identification phase was performed as previously explained, by subjecting a nominal wind turbine model to wind fields of different known mean speed and direction, and recording the associated blade root moments. This nominal observation model was then used for estimating wind misalignments from the response of perturbed wind turbine models, obtained by changing some of the machine parameters with respect to their nominal values. The study considered perturbations in the following model parameters:

- Stiffness of foundations (up to -40% change), on account of different soil characteristics of different installations. Only reductions in the foundation stiffness of the reference virtual model were considered, as higher values did not lead to noticeable changes in the response.

- Vertical inclination of the wind flow (up to ±6 deg with respect to the value used for the identification of the observation model), on account of orographic effects of different installation sites.

- Rotor unbalance due to pitch misalignment of one of the three blades (up to ±0.9 deg).

8

- Miscalibration of one blade load sensor, where bending moment m in the flapwise or edgewise direction is assumed to be sensed as $m_s = c + sm$, c being a constant bias (up to $\pm 0.1\%$ of the bending moment at standstill with the blade parallel to the ground) and s a miscalibration scaling factor (considered to be comprised in the range $s \in [0.9, 1.1]$).

- Changes in the airfoil aerodynamic characteristics (up to 24% increase in drag and up to 24% reduction in lift), on account of effects such as leading edge erosion, dirt accumulation and formation of ice on the blades.

Two wind time histories were considered in the analysis. The evolution in time of the wind speed, misalignment angle and shear coefficient of the first time history are reported in Fig. 1, together with the corresponding blade loads for the nominal model; the second wind time history simply differs in the misalignment angle, which is of the opposite sign. The figure also reports with a dashed line the misalignment observed with the present formulation, based on the response of the nominal model.
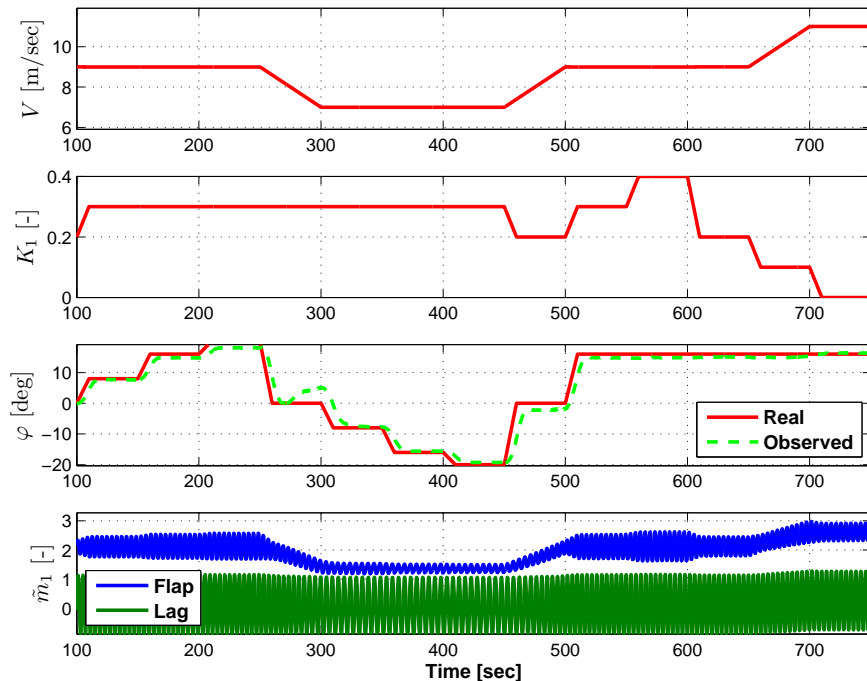

Figure 1: Wind time history for robustness analysis. From top to bottom: rotor averaged wind speed, shear power law coefficient, wind misalignment angle, blade bending moments at root of blade 1 for the nominal wind turbine model.

Simulations were run for all considered perturbation types and intensities, and for both wind time histories. In order to evaluate the robustness of the observation performance with respect to the nominal condition, an

average observation error throughout each simulation was defined as follows

$$\Delta\varphi = \frac{1}{T} \int_T |\varphi^*(t) - \varphi^{\text{real}}(t)| \mathrm{d}t, \tag{9}$$

where $(\cdot)^*$ is an observed quantity, and the time window was defined as $T = t_e - t_i$, with $t_i = 100$ sec and $t_e = 750$ sec, respectively, to exclude initial transients. The average error computed for the pth perturbed case is labelled $\Delta\varphi_p$, while the average error committed under nominal conditions (i.e. when the misalignment observer was operated in conjunction with the same simulation model used for the synthesis of the observation model) is termed $\Delta\varphi_n$. The robustness performance measure for each perturbation type p was finally defined as the following relative increase with respect to the performance of the observer in the nominal case:

$$E_p = \frac{\Delta\varphi_p - \Delta\varphi_n}{\Delta\varphi_n}. \tag{10}$$

The results of the robustness analyses are presented in Fig. 2 that, for each perturbation type and intensity, reports the resulting relative increase in the observation error, after averaging over the two considered time histories (differing in the sign of the misalignment angle).
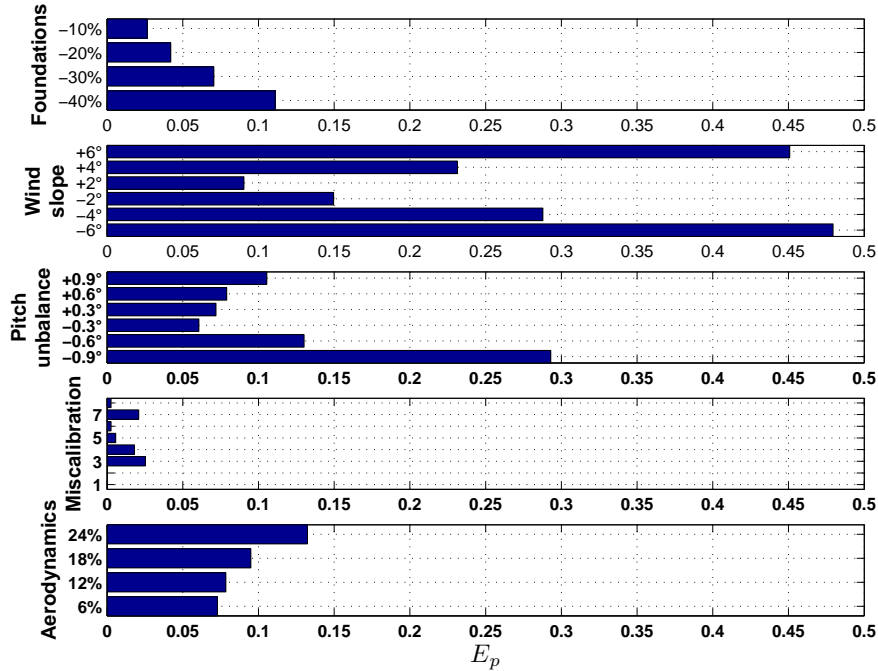

Figure 2: Results of robustness analysis in terms of the average normalized performance metric of Eq. (10). From top: effect of change in stiffness of foundations, wind upflow angle, pitch unbalance, miscalibration parameters, aerodynamic properties of the blades.

The effects of miscalibration were studied through eight reasonable combinations of the bias and sensitivity parameters, but the results show a rather negligible effect of these changes on the results. Similarly, it appears

that in general even considerable perturbations in the various parameters considered here lead to limited increases in the average observation errors. In fact, error increases are usually limited to less than 15%, and actually much less in most of the cases.

Exceptions are found for a pitch unbalance of -0.9 deg, which however is a rather large error as certification guidelines prescribe a value of 0.3 deg [2] for the analysis of the effects of unbalanced rotors, and for changes in upflow angles in excess of about 2 deg. This in fact appears to be the parameter that induces the largest effects on the quality of the observer. This might be taken into account when using the observer on machines located in complex terrains or where the upflow is significant because of the surrounding orography of the terrain.

3. Field testing: methods and results

The misalignment observer described in the previous section was synthesized and tested using data collected on the CART3 wind turbine (see Refs. [3, 4]), a 550 kW, 40 m diameter horizontal-axis three-bladed variable-speed machine developed and operated by NREL's National Wind Technology Center (NWTC). The turbine blades are instrumented with strain gages, while an anemometer and a wind vane are installed in the nacelle. A met-mast, placed at about two diameters upstream of the rotor, provides independent speed and direction information at 15, 36.6 and 58.2 m above ground, roughly corresponding to the rotor lowest, center and top points, respectively. Met-mast and wind turbine on-board measurements are synchronized and sampled at 400 Hz.

3.1. Model identification and RANSAC-based outlier detection

In order to synthesize good quality models using field data, care must be exercised to select and properly use the available samples, as the recorded time histories of wind turbine on-board and met-mast measurements may contain extremely turbulent events, shut-downs and run ups, yawing maneuvers, and other situations that might not be advisable to use in the model identification phase. In fact, the observation model expressed by Eq. (2) is based on the assumption of a periodic response of the machine in steady wind conditions; although wind direction estimates need only capture slowly varying changes in the flow, it is clear that excessively dynamic conditions may negatively affect the model identification phase. Furthermore, it is necessary to assign samples to their relevant mean wind speed buckets, so as to develop a wind scheduled LPV observation model as previously explained.

A two stage procedure was developed to effectively address these problems, that includes a pre-selection of time sequences followed by a RANSAC-type (cf. Ref. [7]) detection of outliers.

The goal of the pre-selection phase is the identification of time sequences of consecutive samples where conditions are sufficiently constant for a sufficient length of time, and to assign them to their respective mean

wind speed buckets. By considering all samples in the set of measurements available for identification, termed $\mathcal{I}$, sequences of samples are first selected according to the following criteria:

- A rotor speed satisfying $\sigma(\Omega)/\bar{\Omega} \leq 5\%$, where $\sigma(\Omega)$ is the rotor speed standard deviation, and $\bar{\Omega}$ the rotor speed average over the considered time sequence.

- A wind misalignment satisfying $\varphi - \bar{\varphi} \in \pm 20$ deg, where $\bar{\varphi}$ is the misalignment average over the considered time sequence. Here again, misalignments were spatially averaged over the three values provided by the met-mast vanes at three different heights above ground.

- Both of the above conditions should be uninterruptedly verified for at least 30 sec.

Time sequences that have passed the above tests are assigned to their corresponding wind speed bucket, if they have a filtered mean wind speed $\hat{V}$ that is at all times within the sequence in the range of ± 1 m/sec with respect to a center-bucket reference wind speed V_k. All samples assigned to bucket k form the sample set $\mathcal{I}_k$. The mean wind speed $\hat{V}$ was obtained by a 5 sec moving average of the average of the three met-mast measurements.

The second stage of the procedure uses a RANSAC algorithm to detect outliers in the sample time histories, trying to identify those samples that for any possible reason are not coherent with the majority of other samples. Notice that no a priori assumption is made on the reason why a given sample should be considered an outlier. The method synthesizes a first model by parameter estimation based on a random set of samples, checks the validity of the model with respect to the rest of available samples according to a given goodness criterion, discards the samples (outliers) that fail to satisfy it, and then repeats the identification with the remaining inliers. By iteratively repeating this process, the procedure tries to find the maximum size set of samples (named consensus set) that, when used for model parameter estimation, satisfies the goodness criterion.

More precisely, for each set of samples $\mathcal{I}_k$ associated with wind speed V_k, the algorithm proceeds as follows:

1. Form a random consensus subset $\mathcal{C}$ of $\mathcal{I}_k$, i.e. $\mathcal{C} = \{\varphi_j, \boldsymbol{m}_j \in \mathcal{I}_k \mid \mathrm{Card}(\mathcal{C}) = N_{\mathcal{C}}\}$. Using $\mathcal{C}$, identify model parameters $\boldsymbol{a}$ using Eq. (7). Here $N_{\mathcal{C}} = 4$ was used, which is the smallest possible value since there are four unknown parameters in the model.

2. Apply the identified observation model to the whole set of load samples $\boldsymbol{m}_i \in \mathcal{I}_k$, which gives all corresponding observed misalignments as $\varphi_i^* = \boldsymbol{a}^T \boldsymbol{m}_i$, $i = 1, \ldots, N_{\mathcal{I}_k}$.

3. For each sample i in $\mathcal{I}_k$, compute the difference between estimate φ_i^* and available met-mast measurement φ_i, $e_i = \varphi_i^* - \varphi_i$, and insert the sample in the consensus set $\mathcal{C}$ if the difference is below a user defined tolerance $e_{\max}$, i.e. $\mathcal{C} = \{\varphi_j, \boldsymbol{m}_j \in \mathcal{I}_k \mid \mathrm{abs}(\varphi_j^* - \varphi_j) \leq e_{\max}\}$.

4. If Card($\mathcal{C}$) has increased with respect to the last iteration, i.e. the consensus is expanding, re-identify new model parameters $\boldsymbol{a}$ with Eq. (7) using the consensus set $\mathcal{C}$, and go to 2, unless a maximum number of iterations has been reached. Otherwise, the consensus is reducing, and the method is re-initialized from step 1 picking a new random set.

Figure 3 plots the inlier ratio Card($\mathcal{C}$)/ Card($\mathcal{I}_k$) vs. wind speed for different values of the threshold $e_{\max}$. It appears that the inlier ratio changes with respect to wind speed, decreasing around rated and at high winds. The low ratio found in proximity of the rated wind speed may be due to the relatively high level of noise that can in general be observed in the machine response around this operating region, at least for the time histories that were available to us for this study. In fact, for winds oscillating just above and below rated, the wind turbine exhibits rapid and rather significant fluctuations in rotor speed and a pronounced control activity. A second reason for the rather low inlier ratio may be due to the quite high turbulence intensity at the installation site [5].

Given the relatively low achievable inlier ratios at wind speeds close to rated, little can be said regarding the actual performance of the proposed observer in this regime, and further investigations are needed with an expanded data set or using another machine. We notice however that the observation algorithm was used successfully in Ref. [1] in simulation studies across the whole wind speed range, including the partial load, transition and full power regions.

The plot also shows that, as expected, more generous error tolerances $e_{\max}$ increase the inlier ratios; based on these results, the value $e_{\max} = 5$ deg was selected for the remainder of the analysis. For this value, relatively good inlier ratios are obtained, except around rated, suggesting a reasonable coherence of informational content amongst the various available measurements.
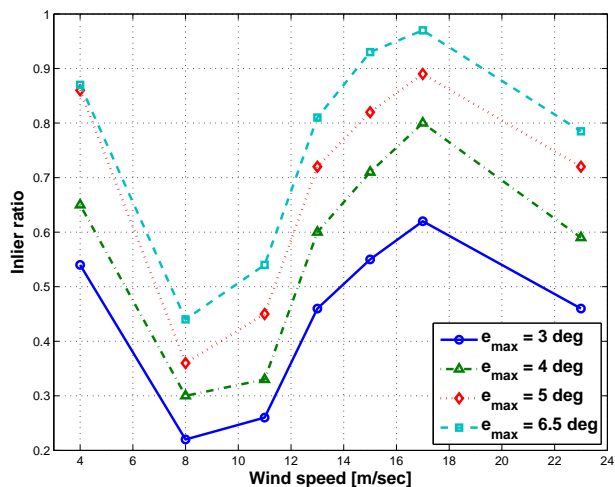

Figure 3: Inlier ratio Card($\mathcal{C}$)/ Card($\mathcal{I}_k$) vs. wind speed for different values of the error threshold $e_{\max}$.

3.2. Observation results

After having identified observation models at each wind speed of interest, as previously explained, their quality was checked against an independent verification data set $\mathcal{V}$, not used during the model estimation phase, i.e. $\mathcal{V} \cap \mathcal{I} = \emptyset$.

The verification data set was subjected to the same pre-selection procedure described for the model estimation data set. Therefore, even in this case, time sequences composed of successive samples were identified for which the rotor speed satisfied $\sigma(\Omega)/\bar{\Omega} \leq 5\%$, the wind misalignment did not change excessively according to $\varphi - \bar{\varphi} \in \pm 20$ deg, and that were of at least 30 sec of duration.

For each time sequence, a mean wind speed estimate $\hat{V}$ was computed by filtering with a 5 sec moving average the average of the three met-mast wind speed measurements. At the generic ith sample, the observation model coefficients were interpolated based on $\hat{V}_i$ using Eq. (8), and the observed misalignments were computed as $\varphi_i^* = \boldsymbol{a}(\hat{V}_i)^T \boldsymbol{m}_i$, discarding the first 5 sec of each sequence on account of the moving average filtering.

A similar criterion used by the RANSAC algorithm was used to detect outliers in the verification set. All computed misalignment estimates and met-mast measurements were processed with a zero-phase fourth-order Butterworth low-pass filter with a cut-off frequency of 1.1 Hz. Next, for each sample, the error between estimates and measurements was determined as $e_i = \varphi_i^* - \varphi_i$, and the sample was classified as inlier if $e_i \leq e_{\max}$, and as outlier otherwise. Similarly, when considering the wind vane time histories, after filtering the error was computed as $e_i = \varphi_i^{\mathrm{wv}} - \varphi_i$, where φ_i^{wv} is the wind vane measured quantity and φ_i the met-mast one, and the sample was classified as inlier if $e_i \leq e_{\max}$, and as outlier otherwise.

In order to account for the delay between measurements collected on the met-mast and on the turbine (in terms of the nacelle wind vane, blade loads and rotational speed), the distance between their respective geographical positions was divided by the mean wind speed. The resulting delay was then used for realigning the time histories.

Two examples of the time histories of observed and measured quantities are presented in Fig. 4. The figure shows the met-mast misalignment using a solid line, the observed value using a dashed line, and the wind vane measurement using a dash-dotted line; all quantities are zero-phase low-pass filtered as explained previously. In both cases, the estimates provided by the proposed observer are well correlated with the met-mast reference, especially at the lower frequencies that are used for wind turbine yaw control. It also appears that the quality of the correlation is much better for the observed misalignments than for the ones measured by the nacelle wind vane.

When comparing these quantities, it should be remembered that met-mast measurements are not a perfect reference. In fact, apart from noise and biases, they only measure the wind direction at three points on the rotor disk. Furthermore, the met mast is located about two diameters away from the wind turbine. This may
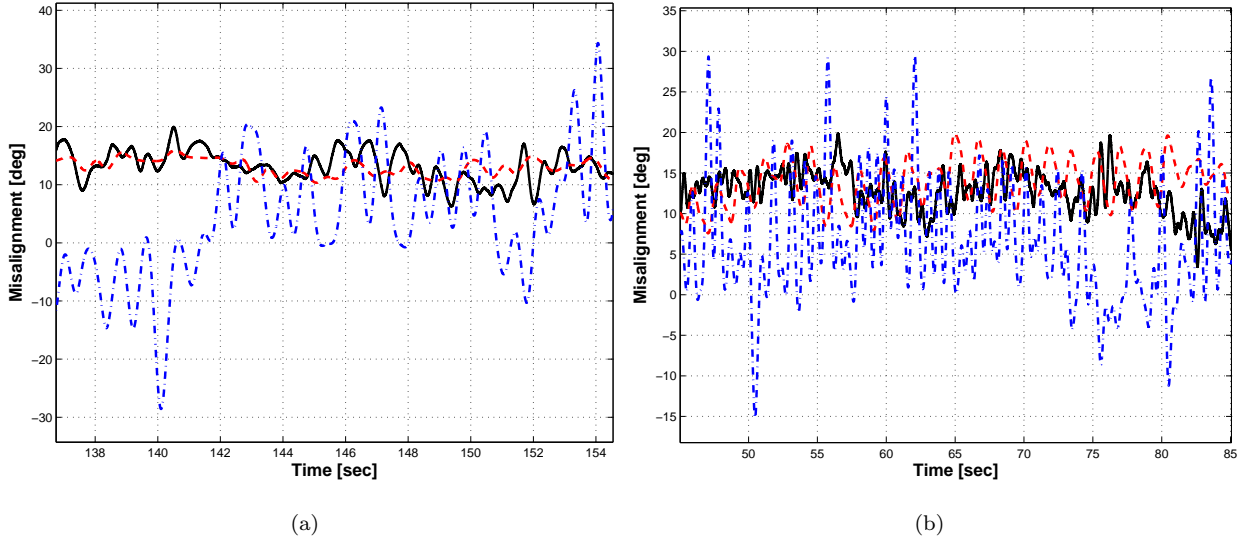
Figure 4: Two wind misalignment time histories, as measured by the met-mast vanes (solid line), by the on-board wind vane (dash-dotted line) and as obtained from the observer (dashed line).

induce errors when the wind direction is not parallel to the turbine/met-mast line, and because the flow does not in general obey Taylor's frozen turbulence hypothesis; even if it did, the correction for the time delay between met-mast and on-board measurements can only be approximate because of the need to estimate a mean transport velocity. Because of these and other reasons, one should keep in mind that met-mast measurements provide for a crucial but imperfect reference.

A coherence measure was used in order to better quantify the similarity of the observations and wind vane measurements with respect to the reference provided by the met-mast vanes. The magnitude squared coherence function C_{xy} (cf. Ref. [16]) between two signals x and y assumes values between 0 and 1 indicating how well the two time histories correspond to each other at any given frequency f, and it writes

$$C_{xy}(f) = \frac{P_{xy}^2(f)}{P_{xx}(f)P_{yy}(f)}, \tag{11}$$

where P_{rs} indicates the power spectral density. The coherence function was estimated using Welch averaged periodogram method (see Refs. [17, 18]); time histories were divided into eight sections of equal length with a 50% overlap, and a Hamming window scheme was applied to each of them.

Figure 5 reports the plots of coherence vs. frequency for the two time histories of Fig. 4. The coherence between observed wind misalignment and met-mast vanes is reported with a dashed line, while the one between wind vane and met-mast vanes using a dash-dotted line. These plots quantify in more precise terms what can be visually perceived from the time histories: the signals are reasonably well correlated at the lowest frequencies (the observer doing better than the wind vane), while for both the correlation rapidly drops at the higher frequencies.
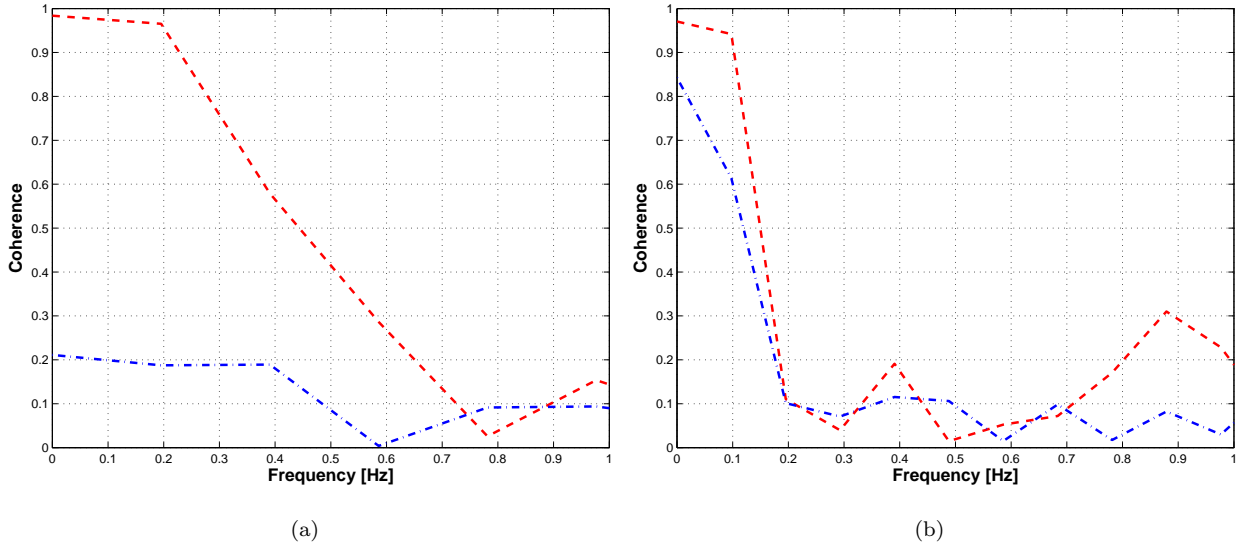
15

Figure 5: Coherence vs. frequency for the time histories of Fig. 4, between observed wind misalignment and met-mast vanes (dashed line), and between on-board wind vane and met-mast vanes (dash-dotted line).

A normalized integral coherence was defined as

$$\tilde{C}_{xy} = \frac{1}{F} \int_0^F C_{xy}(f)\,\mathrm{d}f. \tag{12}$$

This quantity tries to capture with one single scalar the goodness of the coherence between two signals in a frequency band of interest $[0, F]$ Hz. Here the choice $F = 0.25$ Hz was made, as only slow changes of wind direction are typically of interest for yaw control of wind turbines.

Figure 6 reports the normalized coherence for those time histories where all observed filtered misalignment samples were classified as inliers, using an error threshold of 5 deg. These are therefore time sequences where the observed misalignment is reasonably close at all times to the met-mast reference, and the plot tries to compare their quality in terms of coherence with the corresponding on-board wind vane measurements. The normalized coherences between observed and met-mast misalignments are plotted using $*$ symbols, while $\diamondsuit$ symbols indicate normalized coherences between on-board wind vane and met-mast measurements, each pair being connected by a dashed line. As $*$ symbols are consistently and significantly higher in the graph than $\diamondsuit$ symbols, the plot shows that the proposed observer yields results that are most of the time in much better correlation to the ground truth than the on-board wind vane. Notice also that at times the coherence of the on-board wind vane is extremely low, indicating a measurement that is grossly in error with respect to the reference.

Figure 7 reports the normalized coherence for those time histories where all on-board wind vane filtered measurement samples were classified as inliers, using the same error threshold as before. These are therefore time sequences where the on-board wind vane performs relatively well. As for the previous case, normalized
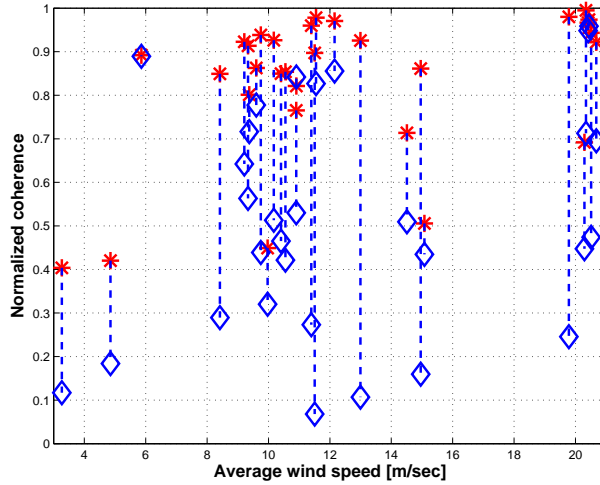
16

Figure 6: Normalized integral coherence $\tilde{C}_{xy}$ vs. average wind speed for time histories where observed misalignments were classified as inliers. Coherence between observed and met-mast misalignments: $*$ symbols; coherence between on-board wind vane and met-mast misalignments: $\diamond$ symbols.

coherences between observed and met-mast misalignments are plotted using $*$ symbols, while normalized coherences between on-board wind vane and met-mast misalignments with $\diamond$ symbols. This second plot shows that when the on-board wind vane provides reliable estimates with respect to the met-mast vanes, the same is largely true for the proposed observer; in addition to this, as the $*$ symbols are generally higher than the $\diamond$ ones, the observer also typically provides for a better coherence and it is therefore more precise. Furthermore, it appears that on average the normalized coherence of the inlier time histories ($\diamond$ symbols in Fig. 7) is much lower than in the previous case ($*$ symbols in Fig. 6), indicating once again a significantly better performance of the observer than the on-board wind vane.

4. Conclusions

A previously described observer of wind misalignment has been tested with the help of experimental data collected in the field on NREL's CART3 wind turbine. The observer uses 1P blade load harmonics to infer the rotor-equivalent wind misalignment. The simple linear structure of the observer is suggested by the analysis of an analytical flapping blade model, while the actual model parameters were here identified using a model-free approach by least squares fitting.

Based on the results of the present investigation, the following conclusions may be drawn:

- The observer appears to be rather robust to changes in some of the wind turbine parameters that may vary among different installations of a same wind turbine version. This seems to indicate that one may calibrate the observer using a met-mast equipped machine, and then use the same observer on-board
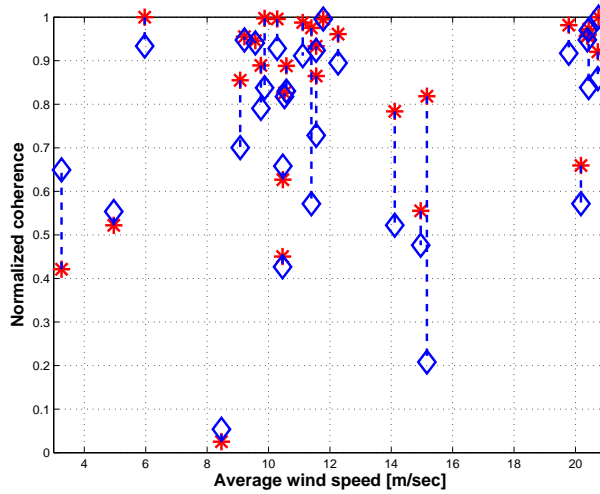
17

Figure 7: Normalized integral coherence $\tilde{C}_{xy}$ vs. average wind speed for time histories where on-board wind vane misalignments were classified as inliers. Coherence between observed and met-mast misalignments: $*$ symbols; coherence between on-board wind vane and met-mast misalignments: $\diamondsuit$ symbols.

other wind turbines of the same version, possibly with no need for re-calibration during the lifetime of each machine.

- The model-free setup of the observer avoids the use of an aeroelastic model of the machine (cf. Ref. [1]), whose possible imperfections may pollute the resulting estimates. On the other hand, the direct estimation of the model parameters from field test data shall be performed with care, given the presence of noise, turbulence and of outliers in the available data due to a large number of possible reasons. A specific two stage procedure was developed in the present paper to cope with these problems, that first pre-selects suitable candidate time histories and then identifies and discards outliers from the samples using a RANSAC-type method. This approach was instrumental for achieving satisfactory identification results.

- The available data sets appeared to be too noisy and turbulent around rated wind speed to allow for a credible verification of the observer in this operating regime. Because of this, it was difficult to identify time sequences of sufficient length where the wind and rotor speed were relatively constant. Additional data sets would be necessary to extend the validation work to this wind speed region, an activity that we hope to perform and report on in the near future.

- In the lower and higher wind speed regime, the available time histories exhibited a better consensus, indicating a coherent informational content within the measurements; in turn, this allowed for the identification of observation models of good quality, covering by wind-scheduling a significant wind

18

speed range. Results obtained with the proposed observer suggest that wind misalignment estimated by blade loads is in general better correlated with the met-mast reference than wind misalignment measured by the on-board wind vane. Time history and coherence plots have shown that the on-board wind vane sensor can at times be grossly in error, possibly because of disturbances due to the nacelle and rotor wake, and also because of the very local point measurement that it performs, all problems that do not affect the proposed observation approach. Furthermore, the accordance between observed and met-mast misalignments is especially good in the lowest band of the spectrum. This is important, because low frequency changes in wind direction are routinely used for driving wind turbine yaw control strategies.

As the CART3 has a relatively small rotor diameter of 40 m, the spatial variability of wind direction over its rotor disk might in general be not too large. Additional investigations on larger machines might further highlight the importance of the rotor-equivalent wind misalignment information provided by the proposed approach, compared to the point local measurements of standard sensors.

Acknowledgments

References

[1] C.L. Bottasso, and C.E.D. Riboldi, Estimation of wind misalignment and vertical shear from blade loads, Renewable Energy 26(2014) 293–302.

[2] Guideline for the Certification of Wind Turbines, Ed. 2010. Germanischer Lloyd Industrial Services GmbH, Renewables Certification, Brooktorkai 10, 20457 Hamburg, Germany (2010)

[3] P.A. Fleming, A.D. Wright, L.J. Fingersh, and J.W. van Wingerden, Resonant vibrations resulting from the re-engineering of a constant-speed 2-bladed turbine to a variable-speed 3-bladed turbine, in: 49th AIAA Aerospace Sciences Meeting, Orlando, Florida, January 4–7, 2011.

[4] E. Bossanyi, P.A. Fleming, and A.D. Wright, Controller field tests on the NREL CART3 turbine, Technical Report 11593/BR/09, 2009.

[5] P.A. Fleming, and K. Kragh, Rotor speed dependent yaw control of wind turbines based on empirical data, in: 50th AIAA Aerospace Sciences Meeting, Nashville, Tennessee, January 9–12, 2012.

[6] R.P. Coleman, and A.M. Feingold, Theory of self-excited mechanical oscillations of helicopter rotors with hinged blades, NACA TN 1351, 1958.

[7] M.A. Fischler, and R.C. Bolles, Random sample consensus: a paradigm for model fitting with applications to image analysis and automated cartography, Communications of the Association for Computing Machinery 24(1981) 381–395.

[8] D.M. Eggleston, and F.S. Stoddard, Wind Turbine Engineering Design, Van Nostrand Reinhold Company Inc., New York, NY, 1987.

[9] T.G. van Engelen, Design model and load reduction assessment for multi-rotational mode individual pitch control (higher harmonics control), in: European Wind Energy Conference (EWEC) 2006, Athens, Greece, February 27–March 2, 2006.

[10] X. Ma, N.K. Poulsen, and H. Bindner, Estimation of wind speed in connection to a wind turbine, Technical report, Technical University of Denmark, 1995.

[11] K.Z. Østergaard, P. Brath, and J. Stoustrup, Estimation of effective wind speed, in: Journal of Physics Conference Series, The Science of Making Torque from Wind (2007) 75(012082).

[12] C.L. Bottasso, and A. Croce, Advanced control laws for variable-speed wind turbines and supporting enabling technologies, Scientific Report DIA-SR 09-01, Dipartimento di Ingegneria Aerospaziale, Politecnico di Milano, Milano, Italy, January 2009.

[13] C.E.D. Riboldi, Advanced control laws for variable-speed wind turbines and supporting enabling technologies, Ph.D. Thesis, Politecnico di Milano, 2012.

[14] O.A. Bauchau, C.L. Bottasso, L. Trainelli, Robust integration schemes for flexible multibody systems, Computer Methods Appl. Mech. Eng. 192(2003) 395–420.

[15] C.L. Bottasso, A. Croce, Cp-Lambda: user's manual, Technical Report, Dipartimento di Scienze e Tecnologie Aerospaziali, Politecnico di Milano, 2006–2013.

[16] S.M. Kay, Modern Spectral Estimation, Prentice-Hall, Englewood Cliffs, NJ, 1988.

[17] L.R. Rabiner, and B. Gold, Theory and Application of Digital Signal Processing, Prentice-Hall, Englewood Cliffs, NJ, 1975.

[18] P.D. Welch, The use of fast Fourier transform for the estimation of power spectra: a method based on time averaging over short, modified periodograms, IEEE Transactions on Audio and Electroacoustics 15(1967) 70–73.